Reordering and synchronization of electrical turbulence in cardiac tissue through global and partial optogenetical illumination

Teng-Chao Li [*]

School of Physics, Hangzhou Normal University, Hangzhou 311121, China
and School of Physics and Telecommunication Engineering, South China Normal University, Guangzhou 510006, China

Wei Zhong and Bao-quan Ai

School of Physics and Telecommunication Engineering, South China Normal University, Guangzhou 510006, China

Wei-Jing Zhu

School of Photoelectric Engineering, Guangdong Polytechnic Normal University, Guangzhou 510665, China

Bing-Wei Li

School of Physics, Hangzhou Normal University, Hangzhou 311121, China

Alexander V. Panfilov [†]

Ural Federal University, Biomed Laboratory, 620002 Ekaterinburg, Russia;
Department of Physics and Astronomy, Ghent University, B-9000 Ghent, Belgium;
and World-Class Research Center "Digital biodesign and personalized healthcare",
I.M. Sechenov First Moscow State Medical University, 119991 Moscow, Russia

Hans Dierckx

KU Leuven Campus Kortrijk–Kulak, Department of Mathematics, Etienne Sabbelaan 53 bus 7657, 8500 Kortrijk, Belgium
and iSi Health - KU Leuven Institute of Physics-based Modeling for In Silico Health, KU Leuven, Belgium

Electrical turbulence in the heart is considered the culprit of cardiac disease, including the fatal ventricular fibrillation. Optogenetics is an emerging technology that has the capability to produce action potentials of cardiomyocytes to affect the electric wave propagation in cardiac tissue, thereby possessing the potential to control the turbulence, by shining a rotating spiral pattern onto the tissue. In this paper, we present a method to reorder and synchronize electrical turbulence through optogenetics. A generic two-variable reaction-diffusion model and a simplified three-variable ionic cardiac model are used. We discuss cases involving either global or partial illumination.

I. INTRODUCTION

Excitable media exist in physical, chemical, and biological systems [1–5]. They possess a stationary rest state resistant to small perturbations, but disturbances above a certain threshold trigger wave propagation [6]. Spiral waves in two-dimensional (2D) medium and scroll waves in three-dimensional (3D) medium are self-sustained excitation waves that can form in these systems. The characteristics of the excitable media may cause spiral or scroll wave instability and breakup due to different mechanisms [7–9]. After that, the interaction of different wavefronts will produce new spiral or scroll waves, making the system more disorganized and resulting in a turbulent pattern [10,11].

Spirals and turbulent patterns in excitable systems attract extensive research due to their connection with cardiac arrhythmia, a medical condition with increasing prevalence worldwide [12]. A normal heartbeat is orchestrated by the stable propagation of the electric wave originating from the sinoatrial node. In the ventricles, the diseased cardiac tissue may block the wave and trigger spiral wave, clinically associated with ventricular tachycardia (VT) [13]. If the excitation waves develop into turbulence, different regions of the heart contract asynchronously and the pumping function is terminated, clinically associated with ventricular fibrillation (VF) [14–16]. It induces the cessation of blood circulation which leads to death within minutes. The most effective therapy for VF is to apply strong electric shocks that rapidly depolarize the cardiac tissue, but this can lead to adverse effects including severe pain and cardiac muscle damage [17,18]. Consequently, low-energy defibrillation techniques have been searched for and analyzed for decades to improve therapies [19–21].

---

[*]Corresponding author: tengchaolee@hznu.edu.cn
[†]Corresponding author: alexander.panfilov@ugent.be

Cardiac optogenetics has recently emerged as a technique for controlling the excitation waves in the heart, which is considered as a way of achieving low-energy defibrillation [22,23]. By using the light-sensitive ion channel channelrhodopsin-2 (ChR2), encouraging advances have been achieved in experimental research. Bruegmann *et al.* terminated ventricular arrhythmias in ChR2 transgenic mouse hearts using epicardial illumination [24]. Nyns *et al.* demonstrated successful VT termination in the rat hearts both *ex vivo* and *in vivo* by apical illumination [25]. Diaz-Maue *et al.* studied whether the illumination of LED arrays can block the spiral waves to terminate arrhythmia in murine hearts *in vitro* [26]. Electric wave control through optogenetics is also studied numerically. Majumder *et al.* used light-induced blocks to drag the spiral wave along a predefined pathway in the monolayers of rat atrial cardiomyocytes [27]. Hussaini *et al.* found that the subthreshold illumination can induce inhomogeneity within cardiac tissue which leads a spiral wave to drift [28]. Xia *et al.* proposed a method to induce directional linear drift of spiral waves under optical feedback through optogenetics [29].

Burton *et al.* achieved reversing the chirality of the spiral wave by a rotating spiral-shaped illumination in the cardiomyocyte monolayers [30]. These results were numerically reproduced and further discussed in our article [31]. Specifically, we found that a rotating spiral-shaped illumination can create a spiral wave in the medium and overwrite the original pattern within two rotation periods.

The ability to overwrite existing excitation patterns with externally induced patterns provides an interesting method for controlling and creating desired excitation patterns, and eliminating unwanted ones in cardiac tissue. However, the application of this methodology to cardiac tissue has several important limitations. In many cases, the light cannot be delivered globally to the entire cardiac tissue, and thus the induced pattern can only be projected onto a part of the heart. Additionally, in the ventricles of the heart, which are essentially 3D, light can only be delivered to the surface of the tissue. As such, it is not clear whether partial illumination will be sufficient to reorder or synchronize the excitation pattern. In this paper, we address these important questions by considering the reordering and synchronization of electrical turbulence in both 2D systems with partial illumination and in 3D excitable media. We perform such studies using a generic two-variable reaction-diffusion model and an ionic model of cardiac tissue and discuss the conditions under which such reordering and synchronization can be achieved.

II. METHODS

A. The generic model

We first combined a generic excitation model with simplified optogenetic coupling.

For the excitable system we used the model of Bär *et al.*[32]:

$$\frac{\partial u}{\partial t} = D\Delta u + \varepsilon^{-1} u(1-u)[u-(v+b)/a] + I_{opto}(x,y,t),$$

(1)

$$\frac{\partial v}{\partial t} = h(u) - v,$$

(2)

with $h(u) = 0$ if $0 \leqslant u < 1/3$; $h(u) = 1 - 6.75u(u-1)^2$ if $1/3 \leqslant u < 1$; and $h(u) = 1$ if $1 < u$. The nonlinear function $u(1-u)[u-(v+b)/a]$ describes an instantaneous depolarizing ionic current. The variable $v(x,y,t)$ mimics a slow repolarizing ionic current, and also accounts for repolarization of the membrane. The function $I(x,y,t)$ describes the ionic current induced through optogenetics and will be explained in detail below. We take $D = 1$, $a = 0.84$, $b = 0.07$, $\varepsilon = 0.075$ and the medium exhibits spatiotemporal turbulence due to the parameters chosen. For numerical simulations, we use a time step $\Delta t = 0.005$ and a grid spacing $\Delta x = \Delta y = 0.2$. We define dimensionless 1 spatial step to be 0.75 mm, such that the wavelength of a spiral wave is 32.25 mm.

In this generic model, we take the electrical current I_{opto} to be instantaneous and proportional to the illumination intensity

$$I_{opto} = 40 I_{light}(\vec{r}, t)$$

(3)

and the illumination pattern to be defined below.

In this study, the illuminated region $\Omega(\vec{r}, t)$ is in the shape of a rotating spiral wave which we copy from an auxiliary spiral wave under the Bär model with parameters $a = 0.84$, $b = 0.07$, and $\varepsilon = 0.05$. This method has been described in detail in our previous work [31].

Here the optogenetics current is simply described as an instantaneous inward current. Whereas our intention is to simulate the action potentials of cardiomyocytes induced by optogenetics and study the subsequent evolution of the wave pattern in the medium, we think such simplification is reasonable for qualitative research.

B. The detailed model

Ionic models that describe cardiac action potential under optogenetics have a basic form of the following reaction-diffusion type equation

$$\frac{dV}{dt} = \nabla \cdot (D\nabla V) - \frac{I_{ion} + I_{ChR2}}{C_m},$$

(4)

where V represents the transmembrane potential, I_{ion} represents the total current flowing through the membrane excluding the ChR2 current, I_{ChR2} is the ChR2 current due to the illumination, C_m is the membrane capacitance, and D is the diffusion coefficient for intercellular coupling. We use a simplified three-current ionic model proposed by Fenton and Karma [33]. The total current is written as

$$I_{ion} = I_{fi}(V; v) + I_{so}(V) + I_{si}(V; w),$$

(5)

where I_{fi} represents the fast inward current, I_{so} represents the slow outward current, and I_{si} represents the slow inward current. v and w are two gate variables that prescribe the dynamics of the currents. By defining a dimensionless variable $u = (V - V_0)/(V_{fi} - V_0)$ and the scaled currents $J = I/(C_m(V_{fi} - V_0))$, where V_0 is the resting membrane potential and V_{fi} is the Nernst potential of the fast inward current, the

TABLE I. Parameter sets of the FK model [9,33]. For both 2D and 3D simulations, we set $C_m = 1\mu$F/cm^2, $D = 0.001$cm^2/ms, $V_0 = -85$mV, and $V_{fi} = +15$mV.

Parameter	2D simulation	3D simulation
τ_v^+	3.33	3.33
τ_{v1}^-	9	1000
τ_{v2}^-	8	19.6
τ_w^+	250	667
τ_w^-	60	11
τ_d	0.3	0.416
τ_0	9	8.3
τ_r	33.33	50
τ_{si}	29	45
k	15	10
u_c^{si}	0.5	0.85
u_c	0.13	0.13
u_v	0.04	0.055

equations of the model can be written as

$$\frac{\partial u}{\partial t} = \nabla \cdot (D\nabla u) - J_{fi}(u; v) - J_{so}(u) - J_{si}(u; w), \quad (6)$$

$$\frac{\partial v}{\partial t} = \boldsymbol{\Theta}(u_c - u)(1 - v)/\tau_v^-(u) - \boldsymbol{\Theta}(u - u_c)v/\tau_v^+, \quad (7)$$

$$\frac{\partial w}{\partial t} = \boldsymbol{\Theta}(u_c - u)(1 - w)/\tau_w^- - \boldsymbol{\Theta}(u - u_c)w/\tau_w^+, \quad (8)$$

where

$$\tau_v^-(u) = \boldsymbol{\Theta}(u - u_v)\tau_{v1}^- + \boldsymbol{\Theta}(u_v - u)\tau_{v2}^-. \quad (9)$$

The three currents are given by

$$J_{fi}(u; v) = -\frac{u}{\tau_d}\boldsymbol{\Theta}(u - u_c)(1 - u)(u - u_c), \quad (10)$$

$$J_{so}(u) = \frac{u}{\tau_0}\boldsymbol{\Theta}(u_c - u) + \frac{1}{\tau_r}\boldsymbol{\Theta}(u - u_c), \quad (11)$$

$$J_{si}(u; w) = -\frac{w}{2\tau_{si}}\left(1 + \tanh\left[k\left(u - u_c^{si}\right)\right]\right). \quad (12)$$

$\boldsymbol{\Theta}(x)$ is the Heaviside step function. The Fenton-Karma (FK) model is a simplified model that is sufficient to reproduce quantitatively the cardiac electrical dynamics and has been extensively used in cardiac modeling research. The parameters used in this paper are shown in Table I. The parameters set in 2D simulations yield a turbulent system due to the Doppler shift, while in 3D simulations, this set of parameters yields a system in which scroll waves have a negative filament tension [9].

The explicit Euler method is used for numerical simulations, with a space step of 0.025 cm and a time step of 0.1 ms. The size of the 2D medium is 10×10 cm^2 and the size of 3D medium is: $12.5 \times 12.5 \times 2$ cm^3. Zero-flux boundary conditions are used for both the generic model and the FK model.

The Fenton-Karma model is here combined with a more detailed optogenetics model proposed by Williams *et al.* that is based on comprehensive experimental data [34]. The optogenetics current is represented as

$$I_{ChR2} = G_{ChR2}G(V)(O_1 + \gamma O_2)(V - E_{ChR2}), \quad (13)$$

with

$$G(V) = [(10.6408 - 14.6408 \times \exp(-V/42.7671))]/V, \quad (14)$$

$$\frac{dC_1}{dt} = G_rC_2 + G_{d1}O_1 - k_1C_1, \quad (15)$$

$$\frac{dO_1}{dt} = k_1C_1 - (G_{d1} + e_{12})O_1 + e_{21}O_2, \quad (16)$$

$$\frac{dO_2}{dt} = k_2C_2 - (G_{d2} + e_{21})O_2 + e_{12}O_1, \quad (17)$$

$$\frac{dC_2}{dt} = G_{d2}O_2 - (k_2 + G_r)C_2. \quad (18)$$

G_{ChR2} is the maximal conductance which is set to 0.4 mS/cm^2. E_{ChR2} is the reversal potential for ChR2, which is set to 0. The conductance ratio γ is set to 0.1. O_1, O_2 are the open-state probabilities, and C_1, C_2 are the closed-state probabilities. The model is modulated by seven kinetic parameters: k_1, k_2, G_{d1}, G_{d2}, G_r, e_{12}, and e_{21}. We set

$$k_1 = 0.8535Fp, \quad (19)$$

$$k_2 = 0.14Fp, \quad (20)$$

$$F = \frac{0.00006\lambda I_{light}}{1.3}, \quad (21)$$

$$\frac{dp}{dt} = (S_0(\theta) - p)/1.3, \quad (22)$$

$$S_0(\theta) = 0.5 \times (1 + \tanh(120(100I_{light} - 0.1))), \quad (23)$$

$$G_{d1} = 0.108, \quad (24)$$

$$G_{d2} = 0.05, \quad (25)$$

$$G_r = 0.004, \quad (26)$$

$$e_{12} = 0.011 + 0.005 \times \log(1 + I_{light}/0.024), \quad (27)$$

$$e_{21} = 0.008 + 0.004 \times \log(1 + I_{light}/0.024). \quad (28)$$

I_{light} is the illumination irradiance. λ=470nm is the wavelength of the light. The illumination intensity is 8.0 mW/mm^2 in 2D and 6.0 mW/mm^2 in 3D.

C. Illumination pattern

In 2D dimensions, the optical intensity is

$$I(x, y, t) = I_{spiral}(x, y, t)[\vec{r} \in \Omega(\vec{r}, t)] \times \boldsymbol{\Theta}(t - t_0), \quad (29)$$

where $I_{spiral}(x, y, t)$ is a rotating spiral shape, as in Ref. [31].

In three spatial dimensions, the illumination exponentially attenuates with the depth in the myocardium [35,36]

$$I(x, y, t) = I_{spiral}(x, y, t)\exp(-z/\delta)[\vec{r} \in \Omega(\vec{r}, t)] \times \boldsymbol{\Theta}(t - t_0). \quad (30)$$

In the 3D graphs below, the z axis points downward from the top side of the medium.
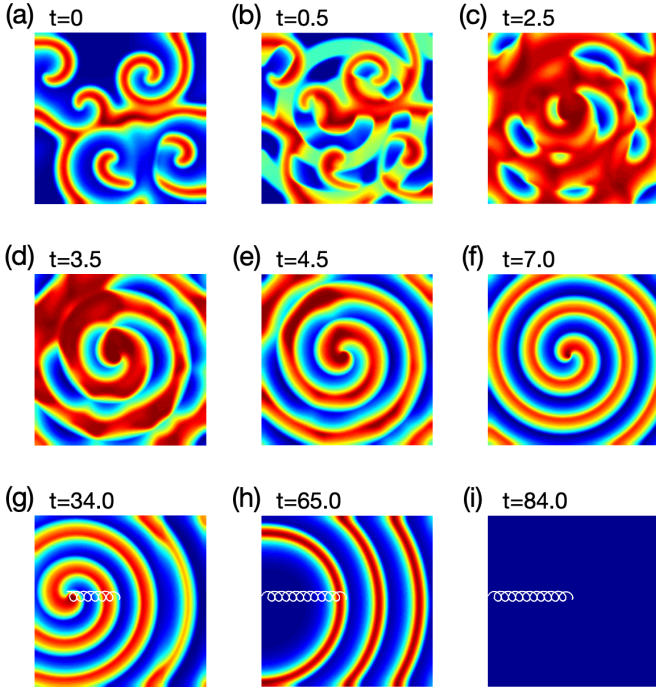
FIG. 1. Reorder and synchronization of 2D spiral turbulence through the rotating spiral-shaped illumination in a homogeneous medium. (a) The initial state. (b)–(f) Evolution when the light is switch on. (g)–(i) Termination of the synchronized spiral by pulling its tip to the edge of the medium through the translation of the rotating illumination. The angular frequency of the light is $\omega_L = 1.51$. The area of the medium is 40×40. Color coding shows the recovery variable v.
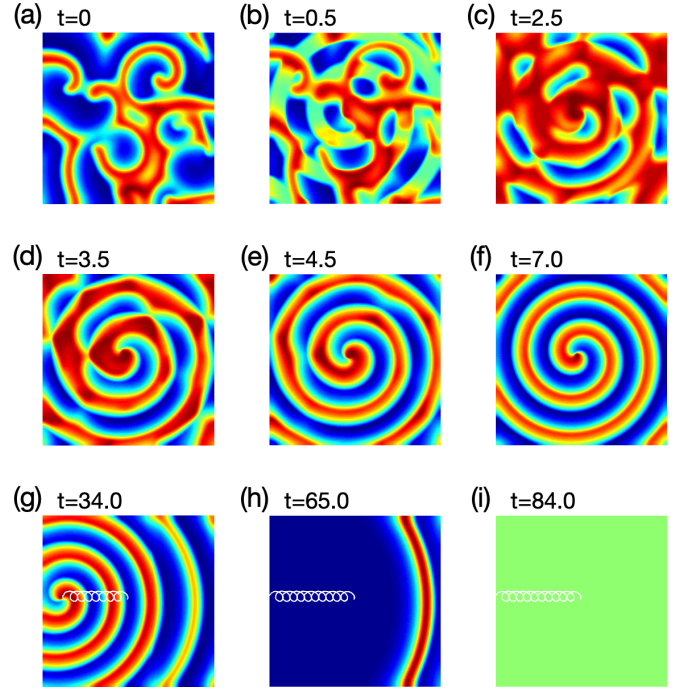
FIG. 2. Achieving reordering and synchronization of 2D spiral turbulence using rotating spiral-shaped illumination in a heterogeneous medium. (a)–(i) A similar scenario shown as described in Fig. 1. The parameter b in Eq. (1) ranging from 0.063 to 0.077 from the left to the right boundary. Other parameters are the same as in Fig. 1. Color coding shows the recovery variable v.

III. RESULTS

Below, we first discuss the synchronization in the generic model, including partial illumination and the 3D case. Then we report if these results still hold in the more detailed model.

A. Synchronization in the generic model

Synchronization and elimination of the spiral. We first report on the optogenetic synchronization in 2D. The original turbulence in Fig. 1(a) is evolved from the breakup of a spiral wave. In Figs. 1(b)–1(f), the rotating spiral-shaped light is continuously applied to the medium. It can be seen in Fig. 1(b) that shortly after the illumination begins, a spiral-shaped region is excited. As the illumination continues, the tips of the initial turbulence disappear [Fig. 1(c)], and the spiral wave is gradually forming [Fig. 1(d)–1(e)]. At the end, the system is dominated by a single spiral wave with the angular frequency as the light. Under these conditions, the center of the rotating light can be moved directly to the boundary along a predefined trajectory. As a result, the tip of the synchronized spiral will follow the moving light and can be easily pulled out of the medium to achieve termination, as shown in Figs. 1(g)–1(i). In this situation, the optogenetics illumination process involves both rotation and translation. The drift speed of the synchronized spiral is determined by the speed of light translation.

Synchronization with spatially varying medium parameters. The elimination of chaos also works in heterogeneous media.

We performed simulations in which we induced a gradient in the threshold of voltage excitation by changing the parameter b in Eq. (1) by 20% from the left to the right boundary. The results are shown in Fig. 2. We see that although heterogeneity results in a different initial pattern of excitation, the control and elimination procedure is identical to what we see in a homogeneous case (see Fig. 1). We think that the success in the inhomogeneous case is realized since the control and elimination are achieved through an externally induced pattern, which is the same in both cases.

Mechanism. Now we will discuss how the illumination suppresses the turbulence and synchronizes the reaction-diffusion system. After the spiral-shaped region has been excited, a refractory tail is formed which hinders the propagation of the original turbulent waves. Since the frequency of the light is close to the dominant frequency of the turbulence, the refractory period will be over before the next arrival of the light, hence the medium will always be excited when being illuminated. Also, when the illuminated region passes through the tip of the original turbulence, the elements around it will be excited and the phase distribution adjacent to the tip is destroyed, resulting in the termination of spiral wave turbulence. Within one or two rotation periods, the system will be dominated by a single spiral wave induced by the illumination. Meanwhile, the wavefront of the spiral is continually stimulated and exciting thereby preventing the spiral breakup while making its angular frequency synchronized with the illumination.
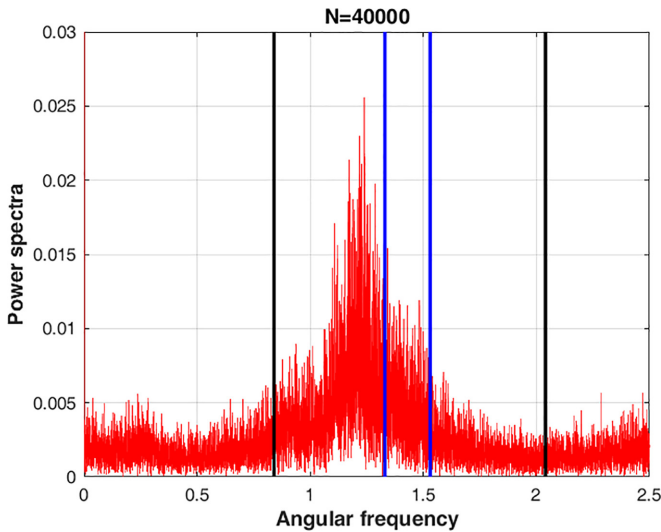
FIG. 3. Power spectrum of the turbulence. The number of data samples is 40 000 and the data sampling frequency is 2. The black lines illustrate the synchronous frequency range of global illumination. The blue lines illustrate the synchronous frequency range of partial illumination.
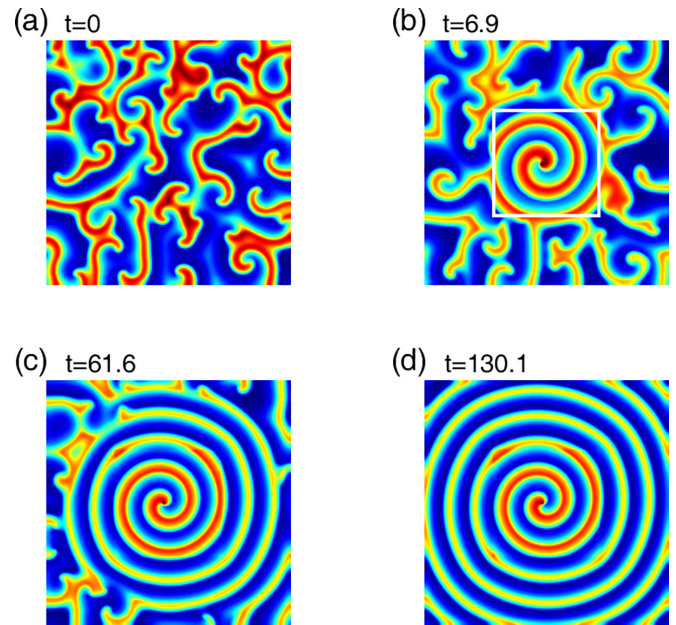

FIG. 4. Synchronization of turbulence through partial illumination. (a) The initial state. (b)–(d) Evolution when the light is switched on. White box represents the illuminated region 30×30. The angular frequency of the light is $\omega_L = 1.46$. The area of the medium is 70×70. Color coding shows the recovery variable v.

We investigate the relationship between the angular frequency of the rotating light and the dominant frequency of the turbulence. Figure 3 shows a typical power spectrum obtained by fast Fourier transformation of a point in the electrical turbulence. We then perform a series of simulations using spiral-shaped light with different angular frequencies, and find that within a specific frequency range indicated by black lines in Fig. 3, the illumination can achieve suppression of the turbulence and synchronize the system. A higher angular frequency will cause the light to catch up with the refractory period left by the previous stimulation. If the angular frequency is too small, the excited wavefront will propagate faster than the illuminated region, causing synchronization failure.

Partial illumination. In many practical situations, global illumination of cardiac tissue is not possible due to technical issues. We therefore studied if partial illumination could reorder the whole system and a successful example is illustrated in Fig. 4. In the illuminated region, the medium evolves into a spiral pattern shortly after the light is turned on. The light-generated waves continue to propagate after passing through the edge of the illuminated area, which is equivalent to generating a periodic incident wave to the peripheral medium. The angular frequency of the incident wave is equal to that of the spiral-shaped light. It has been previously shown that a suitable frequency of incident wave may drive away the turbulence [37,38]. Our results are in good agreement with them as shown in Figs. 4(c)–4(d) that the surrounding turbulence is synchronized by the partial illumination. We find the angular frequency range that accomplishes this synchronization, which is smaller than the range for global illumination, see the blue lines in Fig. 3. One can notice that the synchronization range is slightly above the dominated frequency of the turbulence. The theoretical explanation has been proposed by Pravdin *et al.* [38]. In short, the incident

wavefront collides with the turbulent core at a suitable phase, causing the tip to drift a small distance towards the medium boundary. The tip will continue to curl and collide with the next incident wavefront exactly at that suitable phase within one rotation period. The repetition of this process leads to the synchronization of the turbulence system. In cardiac tissues, the application of partial illumination could be much easier than global illumination. There is a critical minimal value for the partial illumination region, denoted as 5×5 (18.75 mm $\times$ 18.75 mm), beyond which turbulence can be synchronized. This value is significantly smaller than the spiral wave length 32.25 mm.

Synchronization in a 3D medium. Now we discuss the results for the generic model in 3D. Simulations are performed in a $40 \times 40 \times 21$ box, with the same model parameters as in 2D.

We simulate the situations when the light intensity decays rapidly and slowly by setting δ to 3 (11.25 mm) and 5 (18.75 mm), respectively. Figure 5 shows the results when light intensity decays slowly, where the intensity at the bottom of the medium is still enough to synchronize the turbulence as in 2D simulations. In the initial state in Fig. 5, one can see that the filaments are curled and distributed over the box. The filaments become dense shortly after the illumination begins. Most of the filaments occur at the junction of the light-induced wave and the original turbulence segments. By the application of the light, conduction block regions form near the illuminated side, which are seen as filaments. However, since filaments can only end on the medium boundary, they subsequently spread deeper into the medium, as shown in Fig. 5(b). In Fig. 5(d), the upper part of the system, where the light intensity is stronger, has been synchronized since there
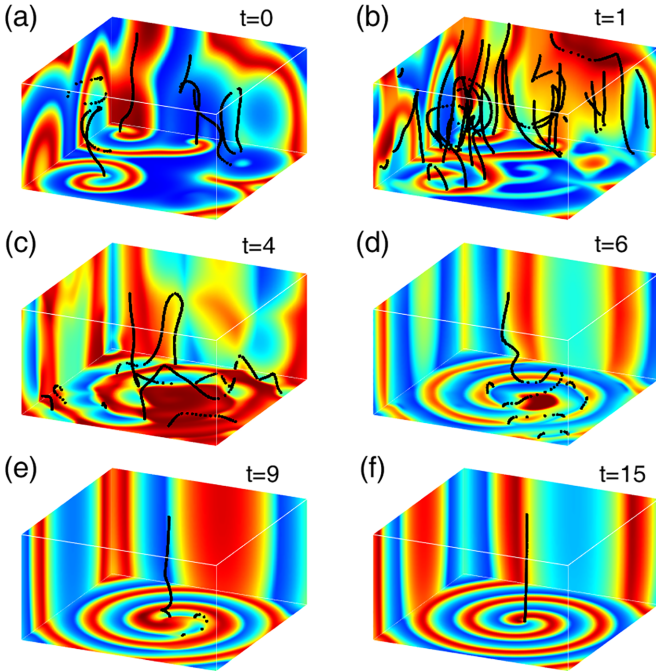
FIG. 5. Synchronization of 3D spiral turbulence through rotating spiral-shaped illumination. The size of the medium is $40 \times 40 \times 21$. The angular frequency of the light is $\omega_L = 1.51$. The attenuation coefficient of light intensity is $\delta = 5$ (18.75 mm). Color coding shows the recovery variable v on the bottom, left, and back faces of the box. The light is shone from above. The filaments are displayed in black to illustrate the excitation waves inside the box. The light intensity is enough to synchronize the turbulence at all depths in the medium.

is only one filament located in the center. The bottom face already shows a rough spiral wave pattern, although there are still some disordered filaments remaining near the bottom. In Fig. 5(f), the whole system has been synchronized to the state of the scroll wave within four rotations of the light.

However, if we decrease the optical penetration depth δ to $\delta = 3$ (11.25 mm) (Fig. 6), only partial synchronization could be achieved, for about 3/5 of the total thickness. However, we still see a substantial decrease in the complexity of the excitation pattern.

One may wonder if our method of partial illumination is still effective in 3D. We demonstrate that our method works with a value of $\delta = 5$ (18.75 mm), as shown in Fig. 7 .

To investigate the effect of the penetration depth δ, we have tracked for the cases of incomplete synchronization the depth D_s until where the filaments remained straight after 200 time units of optical synchronization, see Fig. 8. The relation between D_s and δ turns out to be linear, which tells us that the synchronization is effective up to a depth D_s where the illumination intensity is above $I_{\min} = I_{\text{spiral}} \exp(-z/\delta)$. Under these circumstances, if we use a value of $\delta = 1$ mm, our method could be feasible for synchronizing the thinner right ventricle as well as the atria. When $\delta = 4$ mm, it may be sufficient to synchronize the left ventricle.

Synchronization under noisy conditions. Cardiac tissue and gene expression in gene therapies are strongly heterogeneous. To demonstrate the robustness of our method with

respect to heterogeneities, we add strong spatiotemporal white noise $\sigma(x, y, z, t)$ [39,40] to the right-hand side of Eq. (1), in which $\sigma(x, y, z, t) = 0$, $\langle \sigma(x, y, z, t) \sigma(x', y', z', t') \rangle = \eta \delta(x - x') \delta(y - y') \delta(z - z') \delta(t - t')$, with a noise amplitude of $\eta = 0.03$, which is 10 times higher than that used in Ref. [40]. One can see that, despite the noise, a similar synchronization scenario occurs: compare Fig. 9 and Fig. 5.

B. Synchronization in the detailed model

Synchronization and spiral elimination. The 2D result for the more detailed excitation-optogenetics model is shown in Fig. 10. We set the illumination irradiance $I_{light} = 8.0$ mW/mm^2 in the optogenetics model. The light pattern is the same as in Fig. 1 with its angular frequency $\omega = 62.8$ rad/s. After the illumination begins, a spiral-shaped region is excited [Fig. 10(b)] and its tip is generated [Fig. 10(c)]. The light-induced wave leaves a refractory tail that blocks the original
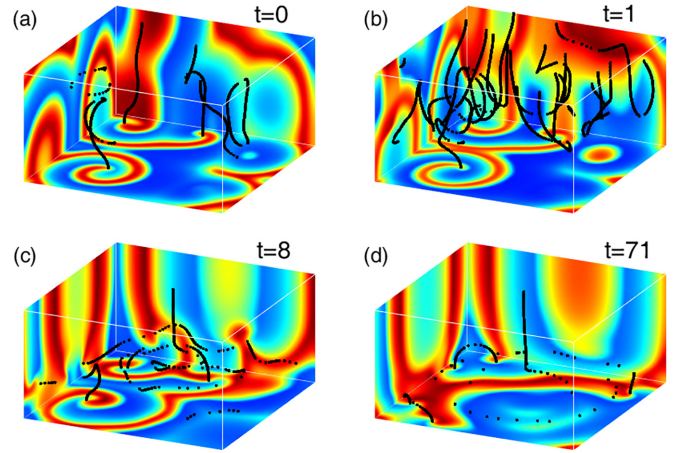

FIG. 6. Evolution of 3D medium when light intensity decays fast. The attenuation coefficient of light intensity is $\delta = 3$ (11.25 mm). Other parameters are the same as in Fig. 5. The light is shone from above. Color coding shows the recovery variable v.
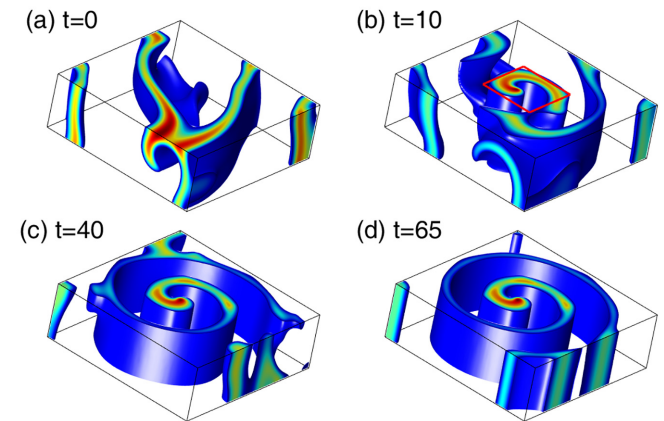

FIG. 7. Stereogram shows the synchronization of 3D turbulence through partial illumination. Simulations are performed in a $30 \times 30 \times 10$ box. Red box represents the illuminated region 10×10. Other parameters are the same as in Fig. 5. The light is shone from above. Color coding shows the recovery variable v.
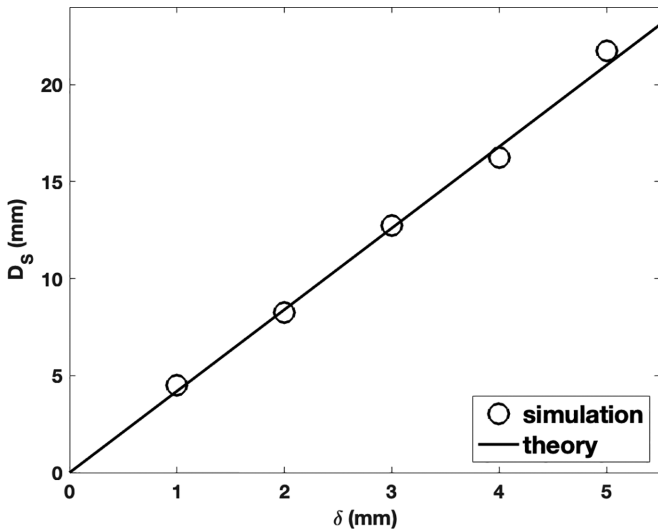
FIG. 8. Synchronization depth D_S as a function of the attenuation coefficient of light intensity δ. Other parameters are the same as in Fig. 5.

FIG. 10. Synchronization of 2D turbulence under Fenton-Karma model through optogenetics. The size of the medium is 10×10 cm^2. The light pattern is the same as in Fig. 1. The angular frequency of the spiral-shaped light is $\omega_L = 62.8$ rad/s. Color coding shows the transmembrane potential V.

turbulence to propagate and dominates the core region. As the illumination progresses, the induced wave gradually dominates the peripheral area. In the final state shown in Fig. 10(f), the light-induced wave has dominated the whole medium and the edges of the wave bands are smoothed. The spiral wave has the same angular frequency as the light pattern, indicating that the system is synchronized. As the light pattern is generated by the generic model, we here demonstrate that a computer generated spiral-shaped light pattern could be efficient when applied to actual cardiac electrical turbulence.

Synchronization in a 3D medium with negative filament tension. We also verify the results in a 3D medium that exhibits negative filament tension. Figure 11 shows the stereograms of the medium. We set the illumination irradiance $I_{light}(z) = 6.0 \times \exp(-z/\delta)$ mW/mm^2. Here we show the results when $\delta = 5$ cm. The stereograms present a clearer view on how the three-dimensional turbulence is synchronized. The
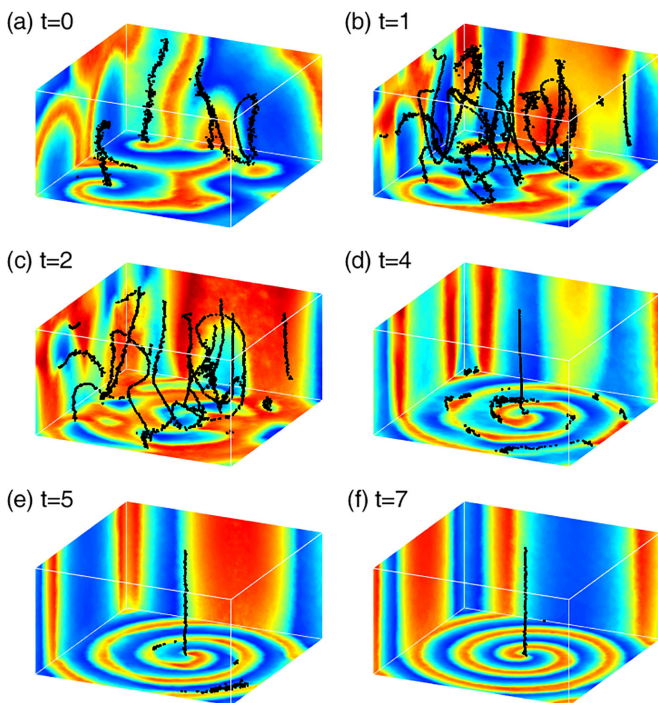

FIG. 9. Synchronization of 3D spiral turbulence achieved through rotating spiral-shaped illumination with a white noise amplitude of $\eta = 0.03$. Other parameters are the same as in Fig. 5. The light is shone from above. Color coding shows the recovery variable v.
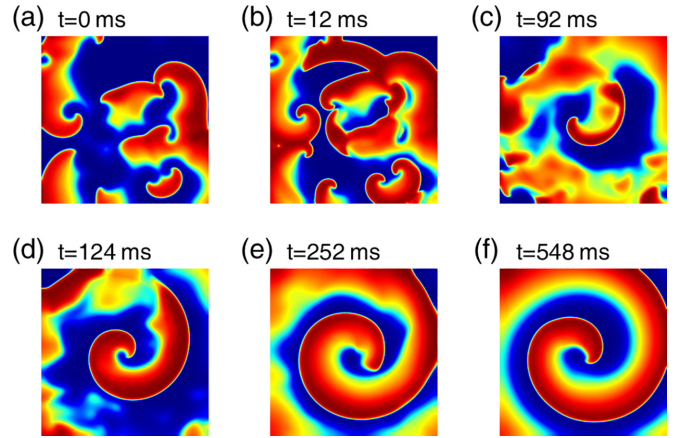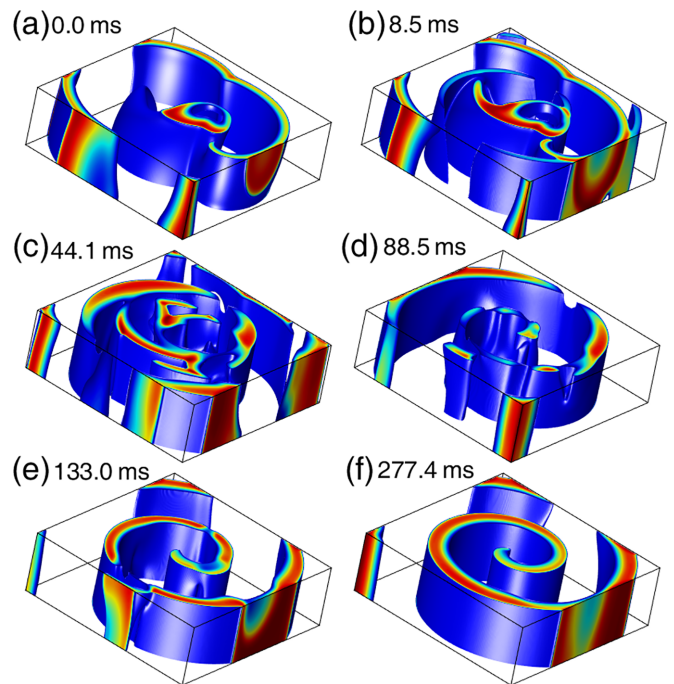

FIG. 11. Stereogram shows the synchronization of 3D turbulence under Fenton-Karma model through optogenetics. The size of the medium is $12.5 \times 12.5 \times 2$ cm^3. The light pattern is the same as in Fig. 1. The angular frequency of the spiral-shaped light is 46.6 rad/s. The light is shone from above. Color coding shows the transmembrane potential V.

spiral-shaped light penetrates the medium, causing an excited region perpendicular to the upper surface, and leaving a refractory wall that suppresses the turbulence. After dominating the medium in Fig. 11(d), the induced waves then evolve into a stable scroll wave which has the same angular frequency with the light as shown in Fig. 11(f). The simulations in the ionic model are consistent with those in the generic model.

IV. DISCUSSION

In this paper we present a method to synchronize the electrical turbulence in cardiac tissue through global and partial optogenetical illumination. We find that the electrical turbulence can be synchronized by rotating spiral-shaped illumination with certain frequencies in both 2D and 3D cases. The synchronization will be continued as long as the illumination does not stop. After synchronization, the spiral or scroll waves can be pulled to the edge of the medium to stop the arrhythmia by directly moving the center of the rotating light. In the cases of 3D, the illumination can synchronize the electric waves within the depth where the intensity of the light is sufficient to synchronize the layer. In this region, the 3D electrical turbulence will be synchronized to a scroll wave.

We convert electrical turbulence into a single spiral or scroll wave. Our rationale is that such spiral waves occur in cardiac tissue and thus converting to such patterns should be more natural. We also tried other excitation patterns, such as single or multiple rotating lines. However, we found that these patterns failed to synchronize turbulence. We did not study in detail the possibility of inducing other excitation patterns, such as concentric circles with various wavelengths. It would be interesting to explore this possibility and also determine whether discrete illumination of the tissue using microLED arrays [41] would be able to synchronize turbulence.

We first used a generic reaction-diffusion model to study the effects of our method, with the optogenetics current set as an instantaneous inward current. We then reproduced these studies in a more detailed model for cardiac tissue with a detailed description of the ChR2 channels to verify the qualitative results. The consistency of the two numerical results demonstrates the feasibility of the simplification.

In our paper, we studied the effect of surface illumination in 3D over a wide range of parameters for the attenuation coefficient δ of light intensity. At its upper limits, it exceeds the attenuation coefficients for currently used optical channels. However, such an extension of the values of the attenuation coefficient is highly expected due to novel methodologies. Recent developments in optogenetics have resulted in the engineering of so-called ultrasensitive optical channels [42]. Those authors showed that such channels can activate neurons located in deep regions of the mouse brain via transcranial optical stimulation. Similar research was recently performed on cardiac tissue, where it was shown that the rat heart can also be excited by transthoracic illumination [43]. Thus, we expect that our simulations, which also involve those with extended light attenuation coefficients, will also describe processes that occur in such systems.

The frequency of illumination should be within a certain range around the dominant frequency of turbulence. Compared to the results of Refs. [37,38], the range of the effective synchronous frequency of our method is much wider. It shows that our method may also be suitable for the system with slight inhomogeneity. Therefore, it is more likely to be realized in more complex real cardiac tissues.

It has been suggested by Winfree that electrical turbulence in the heart muscle is a 3D phenomenon which is induced by negative filament tension [44]. That case is considered in our numerical studies using Fenton-Karma model. The parameters chosen in Fig. 11 will cause the scroll wave breakup due to negative filament tension in 3D, while in a 2D medium, this set of parameters will yield a rigid rotating spiral wave. Our results prove that this kind of 3D electrical turbulence can also be synchronized and will not breakup after the synchronization. It would be interesting to study our approach also for the case of positive filament tension and also possibly develop analytical approaches to this problem, for example, when the drift laws of the filament are simple [45].

In our previous studies, the circularly polarized electric field (CPEF) has been used to order the three-dimensional excitation wave turbulence [46,47]. Furthermore, the results shown in this work suggest that optogenetics methodology could be more efficient to suppress the electrical turbulence.

Recent studies on excitation wave control through optogenetics are mostly around spiral waves, while the more lethal turbulence is rarely studied. Electrical turbulence in cardiac system is fatal due to its disorder, which leads to impaired heart function. Here we demonstrate that a rotating spiral-shaped illumination may synchronize the electrical turbulence in cardiac tissue. That means the cardiac tissue under illumination will be excited orderly, which may terminate the life-threatening VF and restore partial heart function. Noticing that the rotation center of the spiral-shaped light can be chosen arbitrarily, one can find the optimal illuminating position that the heart function can be restored to the greatest extent after the electric excitation wave in the cardiac tissue is synchronized.

In this work, we present a method of global and partial optogenetical illumination in the shape of a rotating spiral wave. It would be interesting to test this in an anatomical geometry of the atria or ventricles in cardiac experiments.

[1] A. M. Zhabotinsky, S. C. Müller, and B. Hess, Physica D **49**, 47 (1991).

[2] K. Agladze, J. P. Keener, S. C. Müller, and A. Panfilov, Science **264**, 1746 (1994).

[3] J. Lechleiter, S. Girard, E. Peralta, and D. Clapham, Science **252**, 123 (1991).

[4] R. A. Gray, A. M. Pertsov, and J. Jalife, Nature (London) **392**, 75 (1998).

[5] S. M. Narayan, D. E. Krummen, and W. J. Rappel, J. Cardiovasc. Electr. **23**, 447 (2012).

[6] E. Meron, Phys. Rep. **218**, 1 (1992).

[7] A. V. Panfilov and A. M. Pertsov, Philos. Trans. R. Soc. A **359**, 1315 (2001).

[8] R. H. Keldermann, K. H. W. J. ten Tusscher, M. P. Nash, C. P. Bradley, R. Hren, P. Taggart, and A. V. Panfilov, Am. J. Physiol. Heart Circ. Physiol. **296**, H370 (2009).

[9] F. H. Fenton, E. M. Cherry, H. M. Hastings, and S. J. Evans, Chaos **12**, 852 (2002).

[10] A. V. Panfilov, Phys. Rev. E **59**, R6251 (1999).

[11] Q. Ouyang, H. L. Swinney, and G. Li, Phys. Rev. Lett. **84**, 1047 (2000).

[12] Cardiovascular diseases Overview on the World Health Organization, http://www.who.int/health-topics/cardiovascular-diseases.

[13] A. M. Pertsov, J. M. Davidenko, R. Salomonsz, W. T. Baxter, and J. Jalife, Circ. Res. **72**, 631 (1993).

[14] A. Karma, Phys. Rev. Lett. **71**, 1103 (1993).

[15] F. X. Witkowski, L. J. Leon, P. A. Penkoske, W. R. Giles, M. L. Spano, W. L. Ditto, and T. Winfree, Nature (London) **392**, 78 (1998).

[16] J. Jalife, Annu. Rev. Physiol. **62**, 25 (2000).

[17] S. F. Sears, J. D. Hauf, K. Kirian, G. Hazelton, and J. B. Conti, Circ. Arrhythm. Electrophysiol. **4**, 242 (2011).

[18] L. Tung, O. Tovar, M. Neunlist, S. K. Jain, and J. O'Neill, Ann. N.Y. Acad. Sci. **720**, 160 (1994).

[19] S. Sinha and S. Sridhar, *Patterns in Excitable Media: Genesis, Dynamics, and Control*, 1st ed. (CRC Press, Boca Raton, 2014).

[20] S. Sinha, A. Pande, and R. Pandit, Phys. Rev. Lett. **86**, 3678 (2001).

[21] S. Luther, F. H. Fenton, B. G. Kornreich, A. Squires, P. Bittihn, D. Hornung, M. Zabel, J. Flanders, A. Gladuli, L. Campoy, E. M. Cherry, G. Luther, G. Hasenfuss, V. I. Krinsky, A. Pumir, R. F. Gilmour, Jr, and E. Bodenschatz, Nature (London) **475**, 235 (2011).

[22] P. M. Boyle, T. V. Karathanos, E. Entcheva, and N. A. Trayanova, Comput. Biol. Med. **65**, 200 (2015).

[23] J. Joshi, M. Rubart, and W. Q. Zhu, Front. Bioeng. Biotechnol. **7**, 466 (2020).

[24] T. Bruegmann, P. M. Boyle, C. C. Vogt, T. V. Karathanos, H. J. Arevalo, B. K. Fleischmann, N. A. Trayanova, and P. Sasse, J. Clin. Invest. **126**, 3894 (2016).

[25] E. C. A. Nyns, T. Y. Jin, M. S. Fontes, T. van den Heuvel, V. Portero, C. Ramsey, C. I. Bart, K. Zeppenfeld, M. J. Schalij,

T. J. van Brakel, A. A. Ramkisoensing, G. Q. Zhang, R. H. Poelma, B. Ördög, A. F. de Vries, and D. A. Pijnappels, Cardiovasc. Res. **118**, 2293 (2022).

[26] L. Diaz-Maue, J. Steinebach, and C. Richter, Front. Physiol. **12**, 750535 (2022).

[27] R. Majumder, I. Feola, A. S. Teplenin, A. A. F. de Vries, A. V. Panfilov, and D. A. Pijnappels, eLife **7**, e41076 (2018).

[28] S. Hussaini, V. Venkatesan, V. Biasci, J. M. R. Sepúlveda, R. A. Q. Uribe, L. Sacconi, G. Bub, C. Richter, V. Krinski, U. Parlitz, R. Majumder, and S. Luther, eLife **10**, e59954 (2021).

[29] Y. X. Xia, X. P. Zhi, T. C. Li, J. T. Pan, A. V. Panfilov, and H. Zhang, Phys. Rev. E **106**, 024405 (2022).

[30] R. A. B. Burton, A. Klimas, C. M. Ambrosi, J. Tomek, A. Corbett, E. Entcheva, and G. Bub, Nat. Photon. **9**, 813 (2015).

[31] T. C. Li, W. Zhong, B. Q. Ai, A. V. Panfilov, and H. Dierckx, Phys. Rev. E **105**, 014214 (2022).

[32] M. Bär, N. Gottschalk, M. Eiswirth, and G. Ertl, J. Chem. Phy. **100**, 1202 (1994).

[33] F. Fenton and A. Karma, Chaos **8**, 20 (1998).

[34] J. C. Williams, J. Xu, Z. Lu, A. Klimas, X. Chen, C. M. Ambrosi, I. S. Cohen, and E. Entcheva, PLoS Comput. Biol. **9**, e1003220 (2013).

[35] P. M. Boyle, J. C. Williams, C. M. Ambrosi, E. Entcheva, and N. A. Trayanova, Nat. Commun. **4**, 2370 (2013).

[36] M. J. Bishop, B. Rodriguez, J. Eason, J. P. Whiteley, N. Trayanova, and D. J. Gavaghan, Biophys. J. **90**, 2938 (2006).

[37] H. Zhang, B. B. Hu, and G. Hu, Phys. Rev. E **68**, 026134 (2003).

[38] S. F. Pravdin, T. V. Nezlobinsky, A. V. Panfilov, and H. Dierckx, Phys. Rev. E **103**, 042420 (2021).

[39] J. Garcia-Ojalvo and J. M. Sancho, *Noise in Spatially Extended Systems* (Springer, New York, 1999).

[40] T. C. Li, D. B. Pan, K. Zhou, R. Jiang, C. Jiang, B. Zheng, and H. Zhang, Phys. Rev. E **98**, 062405 (2018).

[41] N. McAlinden, Y. Cheng, R. Scharf, E. Xie, E. Gu, C. F. Reiche, R. Sharma, P. Tathireddy, M. D. Dawson, L. Rieth, S. Blair, and K. Mathieson, Neurophotonics **6**, 035010 (2019).

[42] X. Gong, D. Mendoza-Halliday, J. T. Ting, T. Kaiser, X. Sun, A. M. Bastos, R. D. Wimmer, B. Guo, Q. Chen, Y. Zhou, M. Pruner, C. W.-H. Wu, D. Park, K. Deisseroth, B. Barak, E. S. Boyden, E. K. Miller, M. M. Halassa, Z. Fu, G. Bi, R. Desimone, and G. Feng, Neuron **107**, 38 (2020).

[43] E. C. A. Nyns, V. Portero, S. Deng, T. Jin, N. Harlaar, C. I. Bart, T. J. van Brakel, M. Palmen, J. Hjortnaes, A. A. Ramkisoensing, G. Q. Zhang, R. H. Poelma, B. Ördög, A. A. F. de Vries, and D. A. Pijnappels, J. Intern. Med. **294**, 347 (2023).

[44] A. T. Winfree, Science **266**, 1003 (1994).

[45] A. V. Panfilov, A. N. Rudenko, and V. I. Krinsky, Biofizika **31**, 850 (1986).

[46] T. C. Li, X. Gao, F. F. Zheng, M. C. Cai, B. W. Li, H. Zhang, and H. Dierckx, Phys. Rev. E **93**, 012216 (2016).

[47] T. C. Li, B. Q. Ai, Y. Chen, and B. W. Li, Phys. Lett. A **388**, 127058 (2021).